Clustering Properties of restframe UV selected galaxies II: Migration of star formation sites with cosmic time from GALEX and CFHTLS

Sébastien Heinis[1,2], Bruno Milliard[1], Stéphane Arnouts[1], Jérémy Blaizot[1,3], David Schiminovich[4], Tamás Budavári[2], Olivier Ilbert[5], José Donas[1], Marie Treyer[1], Ted K. Wyder[6], Henry J. McCracken[7], Tom A. Barlow[6], Karl Forster[6], Peter G. Friedman[6], D. Christopher Martin[6], Patrick Morrissey[6], Susan G. Neff[8], Mark Seibert[6], Todd Small[6], Luciana Bianchi[9], Timothy M. Heckman[2], Young-Wook Lee[10], Barry F. Madore[11], R. Michael Rich[12], Alex S. Szalay[2], Barry Y. Welsh[13], Sukyoung K. Yi[10] and C. K. Xu [6]

ABSTRACT

We analyze the clustering properties of ultraviolet selected galaxies by using *GALEX* - SDSS data at $z < 0.6$ and CFHTLS deep u' imaging at $z \sim 1$. These datasets provide a unique basis at $z \leq 1$ which can be directly compared with high redshift samples built with similar selection criteria. We discuss the dependence of the correlation function parameters (r_0, δ) on the ultraviolet luminosity as well as the linear bias evolution. We find that the bias parameter shows a gradual decline from high ($b_8 \gtrsim 2$) to low redshift ($b_8 \simeq 0.79^{+0.1}_{-0.08}$). When accounting for the fraction of the star formation activity enclosed in the different samples, our results suggest that the bulk of star formation migrated from high mass dark matter halos at $z > 2$ ($10^{12} \leq M_{min} \leq 10^{13} M_{\odot}$, located in high density regions), to less massive halos at low redshift ($M_{min} \leq 10^{12} M_{\odot}$, located in low density regions). This result extends the "downsizing" picture (shift of the star formation activity from high stellar mass systems at high z to low stellar mass at low z) to the dark matter distribution.

Subject headings: Galaxies: UV - Correlation Function Evolution - Star Formation - Downsizing

1. Introduction

Accumulated evidence shows that the cosmic Star Formation Rate (SFR) has been decreasing

[1]Laboratoire d'Astrophysique de Marseille, BP 8, Traverse du Siphon, 13376 Marseille Cedex 12, France

[2]Department of Physics and Astronomy, The Johns Hopkins University, Homewood Campus, Baltimore, MD 21218

[3]Max Planck Institut für astrophysik, D-85748 Garching, Germany

[4]Department of Astronomy, Columbia University, New York, NY 10027

[5]Institute for Astronomy, 2680 Woodlawn Drive, Honolulu, HI 96822

[6]California Institute of Technology, MC 405-47, 1200 East California Boulevard, Pasadena, CA 91125

[7]Institut d'Astrophysique de Paris, Université Pierre et Marie Curie, UMR 7095, 98 bis Bvd Arago, 75014 Paris, France

[8]Laboratory for Astronomy and Solar Physics, NASA Goddard Space Flight Center, Greenbelt, MD 20771

[9]Center for Astrophysical Sciences, The Johns Hopkins University, 3400 N. Charles St., Baltimore, MD 21218

[10]Center for Space Astrophysics, Yonsei University, Seoul 120-749, Korea

[11]Observatories of the Carnegie Institution of Washington, 813 Santa Barbara St., Pasadena, CA 91101

[12]Department of Physics and Astronomy, University of California, Los Angeles, CA 90095

[13]Space Sciences Laboratory, University of California at Berkeley, 601 Campbell Hall, Berkeley, CA 94720

from $z \sim 1$ by a dramatic factor of about 5 (Hopkins 2004; Lilly et al. 1996; Madau et al. 1996; Schiminovich et al. 2005; Sullivan et al. 2000; Wilson et al. 2002). This is linked to the decrease of the contribution of the faint galaxies that dominate the star formation density, and to the strong decline of the most ultraviolet-luminous galaxies with time, given the redshift evolution of the 1500 Å luminosity function (Arnouts et al. 2005). Another aspect of this evolution, known as "downsizing" (Cowie et al. 1996), is the observation that star formation activity shifts with time from high to low stellar mass systems (Bundy et al. 2005; Jimenez et al. 2005; Juneau et al. 2005; Heavens et al. 2004, and references therein).

The star formation history results from the interplay between the physical processes driving the star formation fueling (gas cooling) and regulation (feedback), both closely related to galaxy environment. Recent simulations show that about half of the galaxy gas is accreted through a cold mode, which dominates at high redshift in high density environments, and shifts to low density environments in the local Universe (Kereš et al. 2005). The type of the dominant feedback process is expected to depend on galaxy host halo mass: supernovae explosions (e.g. Benson et al. 2003) at low mass, and AGN (e.g. Croton et al. 2006) at high mass. Cattaneo et al. (2006) show that the introduction of a critical halo mass above which there is a complete shutdown of cooling and star formation is efficient to reproduce the bimodality in galaxy properties observed in the local Universe (e.g. Baldry et al. 2004).

In this paper, we propose to set constraints on the roles of these different processes through cosmic time by assessing the spatial distribution of star formation in the Universe from high to low redshifts. A convenient method is to study the clustering properties of restframe ultraviolet (UV) selected galaxies. This has already been performed at high redshifts using Lyman Break Galaxies (LBGs) samples to show that, at these epochs, star formation is highly clustered and concentrated in overdense regions (Adelberger et al. 2005; Allen et al. 2005; Arnouts et al. 2002; Foucaud et al. 2003; Giavalisco & Dickinson 2001). The study of the redshift evolution of the clustering properties of actively star forming galaxies has now been made possible in a homogeneous way with the combination of restframe UV data collected from $z \sim 4$ to $z = 0$. To extend high-z studies, we use GALEX observations in the recent Universe and CFHTLS deep imaging at $z = 1$. We compute the angular correlation function (ACF) of star forming galaxies and derive their bias and its evolution.

In a companion paper, Milliard et al. (2007, hereafter Paper I), we describe in detail the methodology and the first results of the angular correlation function measurements of UV selected galaxies using a *GALEX* sample at $z \leq 0.6$. Section 2 summarizes the sample properties and presents a new restframe UV-selected sample from the u' band deep CFHTLS imaging survey that we use to extend the analysis to higher redshift ($z \sim 1$). We then investigate the dependence on redshift and UV luminosity of the clustering properties: r_0, δ in sect. 3, bias in sect. 4. In the last section we discuss the evolution of the preferred sites of star formation over the last 90% of the age of the Universe.

All magnitudes have been corrected for Galactic extinction using the E(B-V) value from the Schlegel et al. (1998) maps and the Cardelli et al. (1989) extinction law. Throughout the paper, we adopt the following cosmological parameters: $\Omega_m = 0.3$, $\Omega_\Lambda = 0.7$, $H_0 = 70$ km s^{-1}Mpc^{-1}.

2. Samples description

2.1. *GALEX*

In this work, we use the same subsample of *GALEX* Release 2 (GR2) Medium Imaging Survey (MIS) fields cross-matched with SDSS DR5 presented in Paper I, and we refer to this paper for a full description. We recall here the main characteristics of the selection. We only keep *GALEX* objects with SDSS counterparts within a search radius of 4″and use the closest SDSS match. We select galaxies as objects with SDSS `type` equal to 3. We use the half of the MIS fields from the GR2 dataset with the lowest Galactic extinction ($\langle E(B-V)\rangle \leq 0.04$). Photometric redshifts are computed using an empirical method (Connolly et al. 1995) trained on SDSS spectroscopic counterparts. The standard deviation estimated from the SDSS spectroscopic redshifts is $\sigma = 0.03$. We then use a template fitting procedure (Arnouts & Ilbert, in preparation) to derive

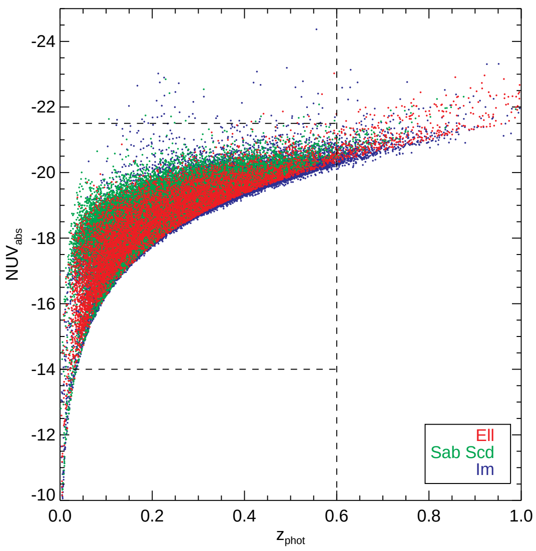

Fig. 1.— NUV absolute magnitude-photometric redshift relation in the $GALEX$ sample. The colors code the type according to the best fitting template: red represent elliptical types, green spirals, and blue irregulars. The dashed lines indicate the additional cuts adopted: $z_{phot} < 0.6$ and $-21.5 < NUV_{\rm abs} < -14$. The same cuts hold for FUV.

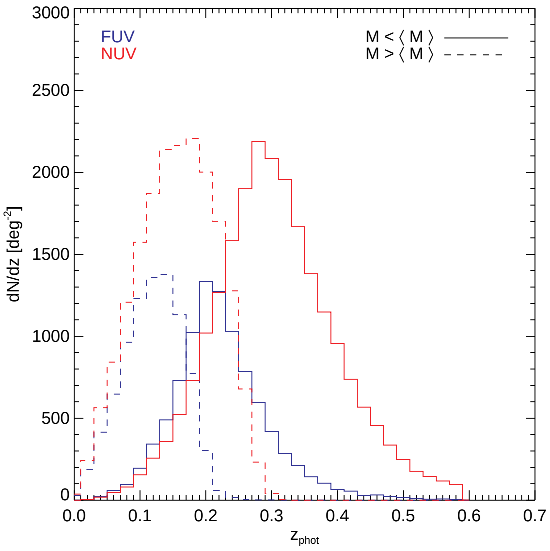

Fig. 2.— Redshift distribution of the subsamples cut in absolute UV magnitude: $M < \langle M \rangle$, solid lines; $M > \langle M \rangle$, dashed lines, FUV is shown as blue and NUV as red.

UV luminosities. Our starting samples include objects with $FUV < 22$ or $NUV < 22$.

The NUV absolute magnitude vs photometric redshift relation is shown in figure 1. The colors code the galaxy type determined using a SED template fitting procedure: red represent elliptical types, green spiral and blue irregular. We restricted hereafter the samples to $-21.5 < NUV_{\rm abs} < -14.$ and $0. < z_{phot} < 0.6$ (dashed lines on fig 1). The same cuts have been applied to the FUV sample.

In the following, we consider both FUV and NUV bands and we divide the samples in two bins according to the mean UV absolute magnitude. The figure 2 shows the photometric redshift distributions of the $GALEX$ samples; the table 1 summarizes the properties of the samples.

2.2. CFHTLS

The CFHTLS-Deep survey consists of deep multi-colour images collected through the $u'g'r'i'z'$ filters over four independent areas of 1 deg^2 each and reaching the limiting magnitude of $i'_{AB} \sim 26$. In this work, we use the official CFHTLS data release T0003. For a full presentation of the CFHTLS-Deep survey, we refer to Schultheis et al. (2006)[1]. We built specific masks from the u-band images to mask out stars, chips edges' and artifacts. The total solid angle of the four fields used after masking is 3.1 deg^2. The star/galaxy separation is based on the same method as McCracken et al. (2003) with the half-light radius versus u magnitude plot. This selection has been applied down to $u = 23$. Beyond this limit, we combine the photometric criterion with the star/galaxy classification derived from the photometric redshift code *Le Phare*, (Arnouts & Ilbert, in preparation).

To construct the sample of UV selected galaxies at $z \sim 1$, we adopt a u' magnitude limit of $u' = 24$, which ensures a genuine UV-selected sample as the u' effective wavelength (3587 Å) corresponds to 1848 Å at our mean redshift $\langle z \rangle = 0.94$. The fraction of objects lost (without any redshift selection) with a $i' = 26$ cut is on average 0.07% over

[1] see also http://www.cfht.hawaii.edu/Science/CFHLS/ and http://www.ast.obs-mip.fr/article204.html

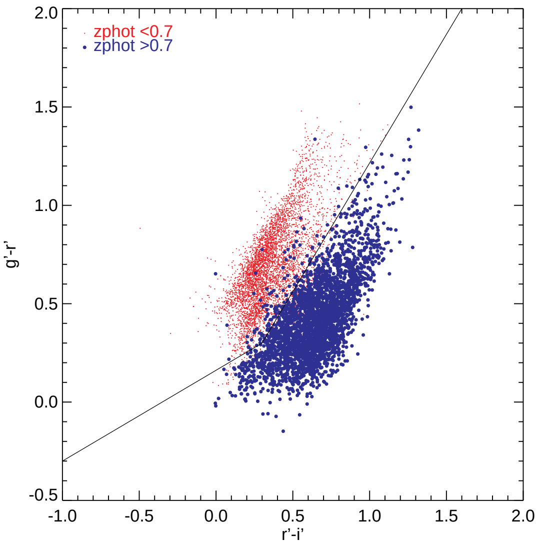

Fig. 3.— Redshift selection based on the $(g' - r')$ vs $(r' - i')$ diagram for the CFHTLS-D1 field. The small dots show galaxies with $z_{phot} < 0.7$ and big dots galaxies with $z_{phot} > 0.7$. The line represents the adopted color-color selection criterion.

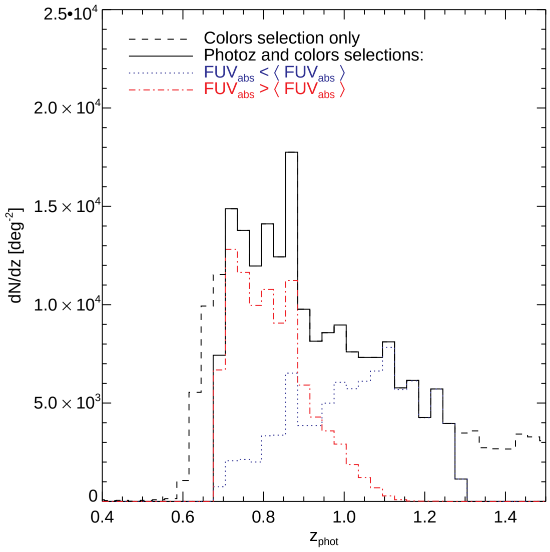

Fig. 4.— Redshift distribution of the CFHTLS sample: the dashed histogram shows the photometric redshift distribution of the galaxies selected with the color criterion alone, while the solid histogram shows the final redshift distribution after selecting objects with $0.7 < z_{phot} < 1.3$. The dotted and dot-dashed histograms show the redshift distributions of the $FUV_{\rm abs} < -19.41$ and $FUV_{\rm abs} > -19.41$ respectively.

the four fields at $u' = 24$. The redshift selection of the sample is based first on a color-color selection and then on the photometric redshift selection. We do not adopt a single selection based on the photometric redshifts because of the variable accuracy of the method due to inhomogeneous exposure times in the five bands for the different fields.

First, we use a color-color selection to isolate galaxies with $z \geq 0.7$, based on VVDS photometric redshifts estimation, relying on multi-color data (Ilbert et al. 2006). As shown in figure 3, the $(g - r)$ versus $(r - i)$ selection criterion is efficient to separate galaxies at $z \geq 0.7$ (big dots) from the lower redshift population (small dots). The line shows our separation criterion. 96% of galaxies with $z_{phot} \geq 0.7$ are located below the line while less than 10% of low z objects ($z_{phot} \leq 0.7$) fall in the same region.

The photometric redshifts are computed by using *Le Phare* code and by adopting the method described by Ilbert et al. (2006). The comparison with the spectroscopic redshifts, obtained by the VVDS in the best photometric field (CFHTLS-D1, Le Fèvre et al. (2005)), for our u' selected sample shows an accuracy of $\sigma(\Delta z/(1 + z)) = 0.03$ with 4% of outliers (defined as $\Delta z \geq 0.15 \times (1 + z)$).

In figure 4 we show the photometric redshift distribution of the galaxies selected with the color criterion (dashed histogram). The final sample is obtained by further selecting objects with $0.7 < z_{phot} < 1.3$ (solid histogram). The absolute magnitudes in the *GALEX* bands are derived from the best fitting SEDs whose NUV-rest flux are well constrained by the u', g', and r' bands in the redshifts range ($0.7 \leq z \leq 1.3$). Note that as the u' filter shifts to *FUV* wavelengths at $z \sim 1$, absolute magnitudes depend very weakly on k-correction and best-fit fitting SEDs. As for *GALEX* samples, we divide the CFHTLS sample in two bins according to the mean *FUV* absolute magnitude and the resulting redshift distributions are shown in Fig 4.

The global properties of the CFHTLS UV samples are given in table 2.

3. Redshift evolution of the correlation function of UV-selected galaxies

We compute the ACF using the Landy & Szalay (1993) estimator. We assume that the ACF is well approximated by a power-law: $w(\theta) = A_w \theta^{-\delta}$; we use a variable Integral Constraint (IC) with δ as free parameter during the power-law fitting process, and estimate the IC with the same method used by Roche & Eales (1999). We derive correlation lengths (r_0) for each sample from the Limber equation (Peebles 1980), using the corresponding redshift distribution. These quantities, as well as the bias parameter[2], are summarized in table 1 and table 2. The effects of the dust internal to galaxies have again been neglected.

In figures 5 and 6, we show the ACFs of the *GALEX* and CFHTLS samples respectively. The ACFs are derived for the global samples and for two sub-samples with UV absolute luminosity brighter and fainter than the mean $< UV_{\rm abs} >$ of each sample. The angular scales probed for the *GALEX* samples are 0.005° to 0.4° (corresponding respectively to comoving distances 0.07 Mpc and 5.7 Mpc at $z = 0.2$), while 0.002° to 0.4° for the CFHTLS samples (resp. 0.11 Mpc and 23 Mpc at $z = 1$). These ACFs are fairly well fitted by power-laws, even if a small dip appears at small scales in the FUV *GALEX* samples and also in the CFHTLS bright one (see sec. 3.2.2). The higher surface density of UV-selected galaxies at $z \sim 1$ allows a less noisy estimation of the ACF at these epochs than at $z < 0.4$.

3.1. Clustering segregation with *FUV* luminosity

The dependence of r_0 on *FUV* luminosity in *GALEX* and CFHTLS samples is shown in fig. 7, along with results from higher redshift studies ($z \geq 2$)[3]. As the different surveys probe different parts of the UV luminosity function with little overlap, it is difficult to draw firm conclusions. Nevertheless, significant differences between the samples are apparent:

- We use as reference the correlation function results from Adelberger et al. (2005), Allen et al. (2005), Foucaud et al. (2003), Giavalisco & Dickinson (2001), Lee et al. (2006) and Ouchi et al. (2001) at $z > 2$. At these redshifts, all studies conclude a significant segregation of r_0 with UV luminosity (the more luminous the more clustered) in the range $-23 \leq FUV_{\rm abs} \leq -20$.
- At $z \sim 1$, a positive correlation of r_0 with *FUV* is still observed for $-20 \leq FUV_{\rm abs} \leq -19$. Notably, our value of r_0 at $FUV_{\rm abs} \sim -20$ is very close to that of Adelberger et al. (2005) obtained from $z \sim 2$ samples.
- At $z \lesssim 0.3$, we probe a fainter luminosity

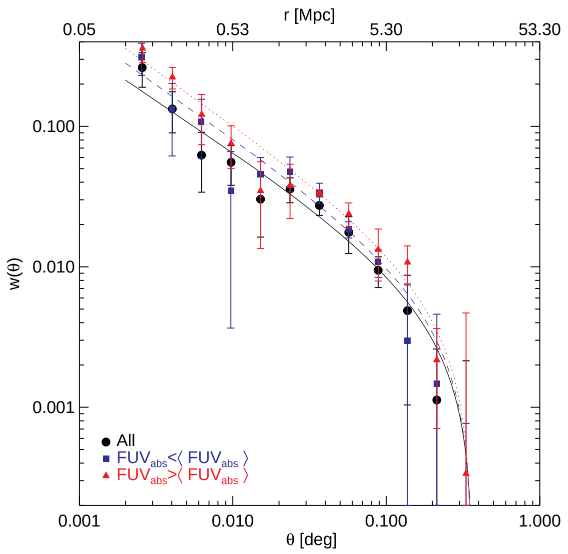

Fig. 6.— Angular correlation function of the CFHTLS subsamples cut in absolute UV magnitude: $M < \langle M \rangle$, squares; $M > \langle M \rangle$, triangles and for comparison the total sample (circles). The curves show the best fit power-laws with the Integral Constraint correction terms subtracted. The upper axis shows the comoving scales corresponding to angular scales at $z = 0.9$.

[2]See Paper I for details on the computations.

[3]We choose the *FUV* absolute magnitude for the comparison as most of high redshift samples are *FUV* restframe selected, and *GALEX* results are not strongly dependent of the UV band.
The mean absolute magnitudes of the LBG samples have been obtained by deriving an average apparent magnitude from the galaxy counts, and assuming a k-correction of $2.5 \log(1 + z)$. Ouchi et al. (2005) do not provide their counts, so we computed the expected mean absolute magnitude given their limiting absolute magnitude and the luminosity function of Sawicki & Thompson (2006).

Table 1

GALEX samples description, power-law best fits parameters, comoving correlation lengths and bias.

	FUV samples			NUV samples		
	All	$FUV_{\rm abs} < -18.3$	$FUV_{\rm abs} > -18.3$	All	$NUV_{\rm abs} < -18.8$	$NUV_{\rm abs} > -18.8$
$N_{gal}{}^{*}$	42065	22082	19983	97038	52567	44471
$\langle FUV_{\rm abs}\rangle$	-18.3	-18.96	-17.57	-18.23	-18.76	-17.61
$\sigma_{FUV_{\rm abs}}$	0.91	0.52	0.67	0.96	0.72	0.82
$\langle NUV_{\rm abs}\rangle$	-18.58	-19.15	-17.95	-18.8	-19.43	-18.05
$\sigma_{NUV_{\rm abs}}$	0.84	0.52	0.67	0.91	0.44	0.69
$\langle z\rangle^{\dagger}$	0.18	0.23	0.13	0.25	0.32	0.17
$\sigma_z{}^{\dagger}$	0.08	0.07	0.05	0.11	0.09	0.06
n_{gal} $[10^{-2}{\rm Mpc}^{-3}]$	2.78±1.03	0.15±0.03	2.54±0.95	2.16±1.19	0.14 ±0.03	1.95± 1.06
$A_w \times 10^3$	$9.4^{+2.4}_{-1.7}$	$7.3^{+3.4}_{-2.2}$	$33.9^{+17.4}_{-10.3}$	$3.6^{+0.6}_{-0.5}$	$4.1^{+1.0}_{-0.8}$	$22.4^{+5.7}_{-4.6}$
δ	0.74±0.05	0.79±0.1	0.48±0.09	0.86±0.04	0.87±0.05	0.52±0.05
r_0 [Mpc]	$4.6^{+0.6}_{-0.5}$	$4.6^{+0.9}_{-0.7}$	$5.4^{+1.5}_{-1.0}$	$4.1^{+0.3}_{-0.3}$	$4.9^{+0.4}_{-0.4}$	$5.5^{+0.8}_{-0.7}$
b_8	$0.74^{+0.08}_{-0.07}$	$0.76^{+0.13}_{-0.1}$	$0.83^{+0.17}_{-0.12}$	$0.69^{+0.05}_{-0.05}$	$0.83^{+0.07}_{-0.07}$	$0.86^{+0.09}_{-0.07}$

*Number of galaxies in the samples

†according to photometric redshifts

Note.—The amplitude and slope of best fit power laws to the angular correlation function, and hence the comoving correlation length account for the Integral Constraint correction, as described in Paper I.

Table 2

CFHTLS samples description, power-law best fits parameters, comoving correlation lengths and bias

	All	$FUV_{\rm abs} < -19.41$	$FUV_{\rm abs} > -19.41$
$N_{gal}{}^{*}$	17098	8507	8591
$\langle FUV_{\rm abs}\rangle$	-19.41	-19.89	-18.94
$\sigma_{FUV_{\rm abs}}$	0.6	0.34	0.36
$\langle NUV_{\rm abs}\rangle$	-19.81	-20.19	-19.43
$\sigma_{NUV_{\rm abs}}$	0.53	0.4	0.33
$\langle z\rangle^{\dagger}$	0.94	1.04	0.84
$\sigma_z{}^{\dagger}$	0.16	0.15	0.09
n_{gal} $[10^{-3}{\rm Mpc}^{-3}]$	3.27±2.90	0.62±0.41	2.66±2.58
$A_w \times 10^3$	$2.7^{+1.4}_{-1.0}$	$2.8^{+1.2}_{-0.8}$	$3.3^{+1.0}_{-0.7}$
δ	0.7 ± 0.09	0.74 ± 0.09	0.76 ± 0.07
r_0 [Mpc]	$4.92^{+0.5}_{-0.5}$	$5.48^{+0.5}_{-0.5}$	$4.66^{+0.24}_{-0.23}$
b_8	$1.24^{+0.08}_{-0.07}$	$1.38^{+0.06}_{-0.07}$	$1.16^{+0.03}_{-0.04}$

*Number of galaxies in the samples

†according to photometric redshifts

Note.—Same note as in table 1

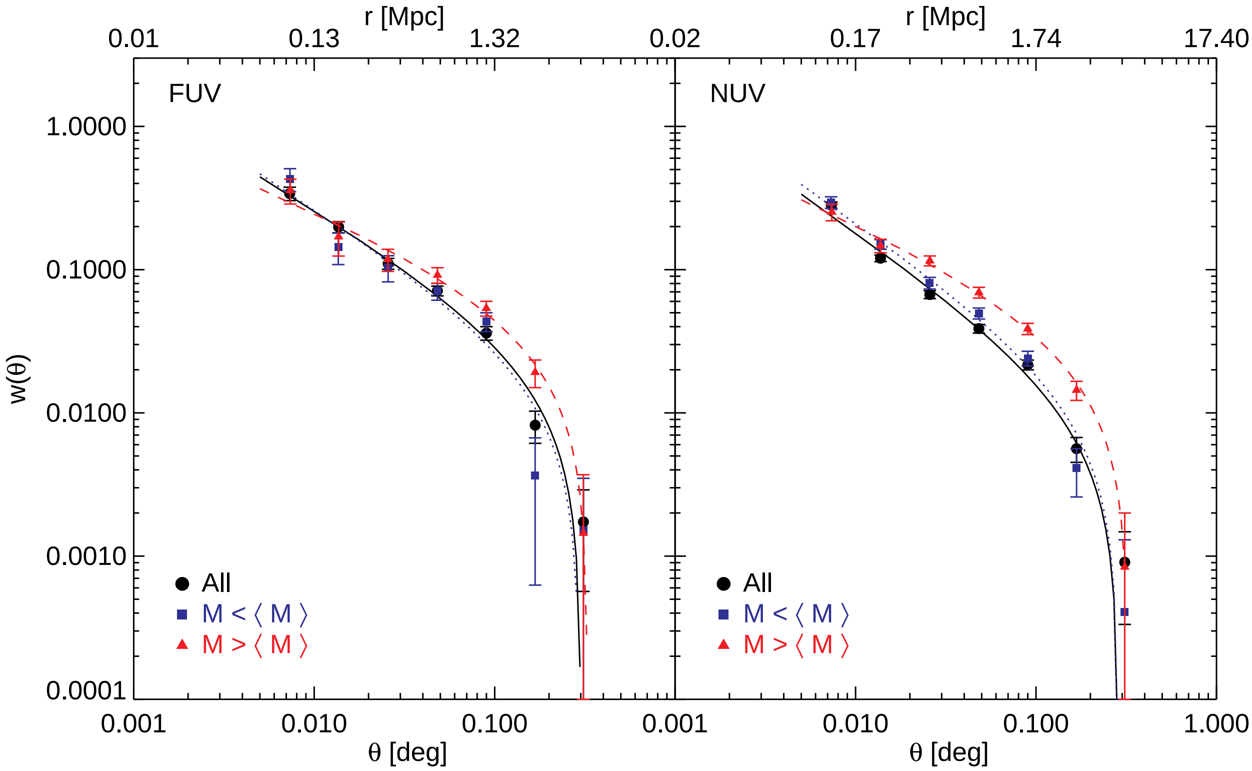

Fig. 5.— Angular correlation function of the *GALEX* subsamples cut in absolute UV magnitude: $M < \langle M \rangle$, squares; $M > \langle M \rangle$, triangles and for comparison the total sample (circles). Left panel, *FUV*; right panel, *NUV*. The curves show the best fit power-law not corrected for the Integral Constraint bias. The upper axis shows the comoving scales corresponding to angular scales at $z = 0.18$ (left) or $z = 0.24$ (right).

range ($-19 \leq FUV_{\rm abs} \leq -17$), and a weak anti-correlation of r_0 with *FUV* is apparent, though given the error bars, it is compatible with no *FUV* luminosity segregation of r_0.

The values of r_0 as a function of *FUV* luminosity for *FUV* selected samples at different redshifts follow a unique smooth curve, with a significant slope at the bright end $FUV_{\rm abs} \leq -19$ and a flat or slightly negative slope at the faint end. A similar segregation is observed with B luminosity at low redshift, with optical selection criteria (Benoist et al. 1996; Guzzo et al. 2000; Norberg et al. 2002; Willmer et al. 1998; Zehavi et al. 2005). In particular, Norberg et al. (2001) showed that for blue-selected galaxies r_0 increases only slowly for galaxies fainter than L_*^B, while it varies strongly for galaxies brighter than L_*^B. Indeed, using N-body simulations Benson et al. (2001) showed that L_*^B could be a natural boundary in the distribution of the halos hosting galaxies, galaxies fainter than L_*^B being hosted by a mix of low and high mass halos, while galaxies brighter than L_*^B hosted by more and more massive haloes. To check if FUV_* could play a similar role in UV samples, we show in figure 8 r_0 as a function of $\langle FUV_{\rm abs} \rangle - FUV_*$, where the evolution of FUV_* with z is taken from Arnouts et al. (2005) (for $z < 1$) and Sawicki & Thompson (2006) (for $z > 1$). The luminosity dependence of r_0 changes noticeably when expressed as a function of $FUV_{\rm abs} - FUV_*$, as two different trends are observed according to the redshift range:

- At $z \geq 1$, for the high z samples and our CFHTLS sample, the behavior of r_0 with $FUV_{\rm abs} - FUV_*$ is qualitatively compatible with the monotonic trend described above,

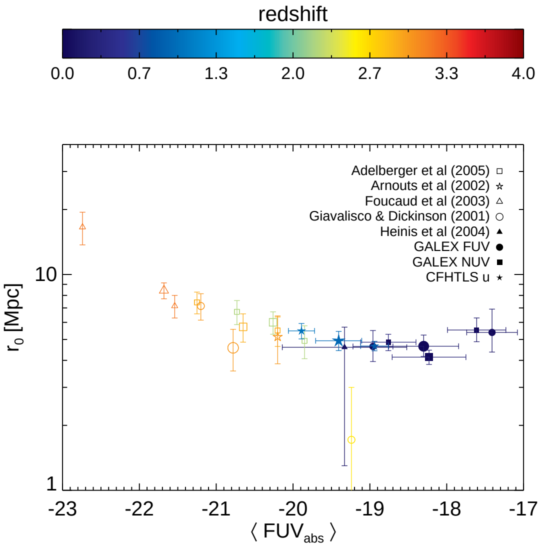

Fig. 7.— Dependence on absolute FUV magnitude of the correlation length r_0 for low and high redshift restframe UV-selected galaxies: open squares, Adelberger et al. (2005); open star, Arnouts et al. (2002); open triangles, Foucaud et al. (2003); open circles, Giavalisco & Dickinson (2001). Our results are presented as filled circles (FUV) and filled squares (NUV) for the *GALEX* samples and as filled stars for the CFHTLS samples. The mean redshifts of the samples are color-coded. Note that the results from a given study (including ours) are not all obtained from independent samples. Hence we distinguish global samples by plotting them with a bigger symbol size, in this figure and in the following ones as well, unless otherwise stated.

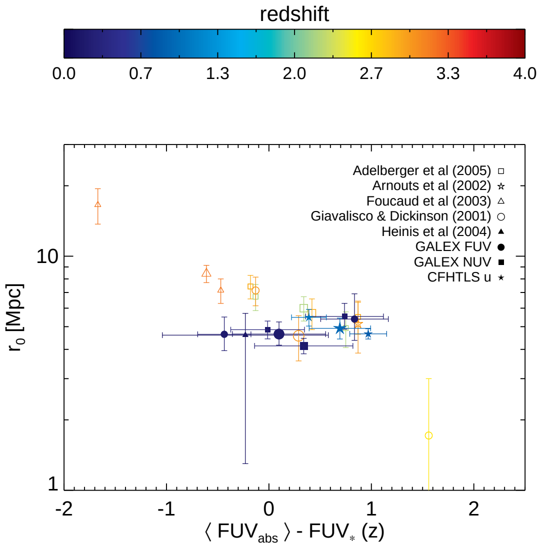

Fig. 8.— Same as in figure 7 but versus $FUV_{\rm abs} - FUV_*$.

the brighter galaxies being more clustered.

- At $z \leq 0.5$ (*GALEX* samples) a radically different behavior of r_0 vs $FUV_{\rm abs} - FUV_*$ is seen. An anti-correlation or no correlation (given the errorbars) is observed, with brighter samples showing slightly lower r_0 than fainter ones.

This suggests that the luminosity segregation mechanisms of the clustering at low redshifts work in a different regime, or that FUV_* is not the relevant variable.

3.2. ACF slope segregation with FUV luminosity

3.2.1. ACF slope

The slope of the ACF (δ), which describes the balance between small and large scale separations, is an important indicator on the nature of the spatial distribution of a given population. In paper I, we found that the estimates of the slope inferred from the global *GALEX* samples ($\delta \simeq 0.81 \pm 0.07$) are steeper than those derived from optically selected blue galaxies in the local Universe: $\delta \sim 0.6$ (Budavári et al. 2003; Madgwick et al. 2002; Zehavi et al. 2002, 2005).
In figure 9, we now analyse the dependence of δ on UV luminosity for the different samples (*GALEX* samples: filled circles for FUV and filled squares for NUV; CFHTLS samples: filled triangles; high z samples: empty squares, open circles and crosses; all points color-coded with redshift).

At $z > 3$, the compilation of measurements showed here, and especially those at at $z = 4$, from Ouchi et al. (2005) indicate that the ACF slope steepens at higher UV luminosities.

Ouchi et al. (2005) claimed that this trend, well modeled in the Halo Occupation Distribution

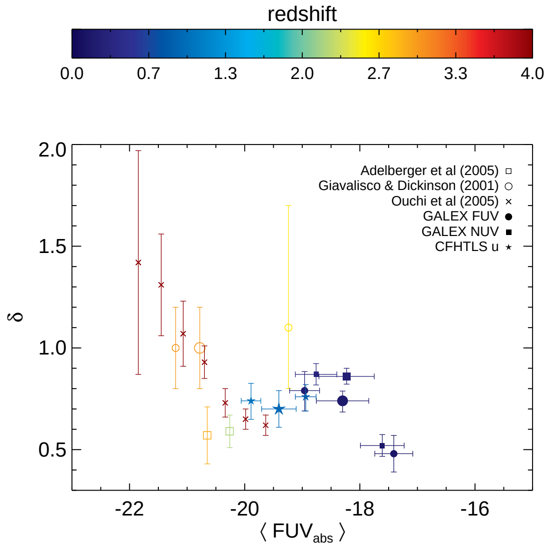

Fig. 9.— Dependence on absolute FUV magnitude of the slope δ of the correlation function for low and high redshift restframe UV-selected galaxies. Results shown here come from studies allowing δ as a free parameter: open squares, Adelberger et al. (2005); open circles, Giavalisco & Dickinson (2001); crosses, Ouchi et al. (2005) (results from the fit with Integral Constraint). Our results are presented as filled circles (FUV) and filled squares (NUV) for the $GALEX$ samples and as filled stars for the CFHTLS samples; the error on δ comes from the fitting procedure and the horizontal bars for our samples reflect the standard deviations of $FUV_{\rm abs}$. The mean redshifts of the samples are color-coded.

(HOD) framework, is not an actual slope variation but it is related to the halo occupancy. Based on HOD models, they show that the contribution of satellite galaxies ('one halo term', see e.g. Zehavi et al. (2004)) increases when selecting brighter galaxies, by enhancing the small scale signal of the ACF ($r \lesssim 0.35$ Mpc). This effect produces an apparent steepening of the observed slope δ.
Our GALEX sample at $z < 0.4$ seems to produce a similar although less pronounced effect. Our current low z GALEX data do not allow to perform detailed comparison between observations and HOD models, but we have investigated if the observed steepening with luminosity can be partially due to the small scale component. We fitted the GALEX ACF only at scales $r > 0.4$ Mpc (see sec. 3.2.2) or $r > 0.7$ Mpc in order not to include the one halo term component. We do not observe any significant change with respect to our initial slopes. However doing so we face at large scales the problems of lower signal-to-noise ratio and more important contribution of the Integral Constraint bias that prevent us to make firm statements. This test thus relies on the efficiency of our power law fitting process in recovering the true ACF (see Paper I).
In other words, at low redshift, we do not see evidence that the one halo term plays a major role in the slope of the ACF, as observed at high redshift, which is expected from simulations (Kravtsov et al. 2004). Hence this indicates that our clustering parameters (r_0, δ and bias, b_8) reflect the large scale clustering of star forming galaxies, which enables us to make comparisons with analytical predictions for the clustering of Dark Matter Haloes.

3.2.2. Dip in the ACF ?

The ACFs derived for the various *GALEX* and CFHTLS samples are globally well described by a power-law, but some of our ACFs show a little dip around 0.35 Mpc, the *GALEX FUV* ones for instance, and also the brightest CFHTLS sample at $z \sim 1$ (at a slightly larger scale ~ 0.5 Mpc). This recalls the departure to the power-law observed in other surveys and interpreted as the transition between the one and two halo terms in the HOD framework. Zehavi et al. (2004) showed that this transition occurs at $\sim 1.5 - 3$ Mpc for r-band selected galaxies. It is expected that this scale should be shorter for bluer galaxies, residing in less massive halos, as showed by Magliocchetti & Porciani (2003) in observations and Berlind et al. (2003, see their fig. 22) in simulations, with a transition scale for late-types galaxies at ~ 0.45 Mpc, close to what we observe. Finally and very interestingly Ouchi et al. (2005) observe this transition for LBGs at $z \sim 4$ at 0.35 Mpc, the same comoving scale as we get.

Comparing measurements with predictions from HOD models is a natural perspective of this work, to probe the redshift evolution of the halo occupancy of star-forming galaxies. This will be addressed in details in a forthcoming paper with enlarged datasets.

4. Bias of star-forming galaxies from $z = 4$ to $z = 0$

The link between the properties of the galaxy distribution and the underlying Dark Matter density field can be accessed via the bias formalism. The bias parameter is indicative of the masses of the dark matter halos that preferentially host the observed galaxy population (e.g. Giavalisco & Dickinson 2001; Mo & White 2002; Ouchi et al. 2004), *i.e.* in our case, actively star forming galaxies. The DM halo bias is a direct output of Mo & White (2002) models. For galaxies, we assume a linear bias to convert r_0 in $\sigma_{8,g}$, a common, though questionable, assumption (see e.g. Marinoni et al. 2005).

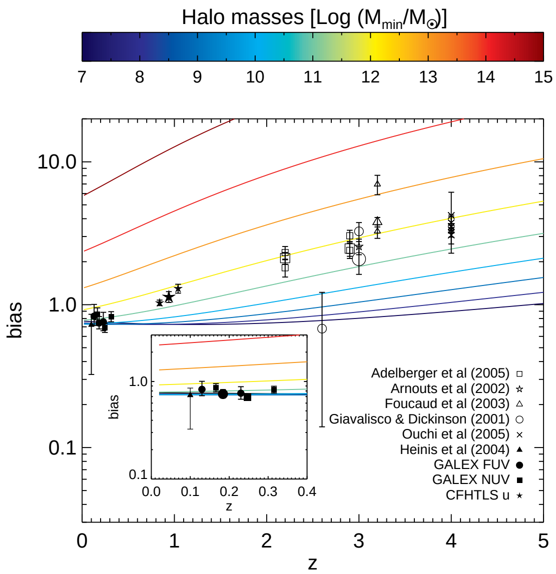

Fig. 10.— Evolution with redshift of the bias of rest-frame UV-selected galaxies (symbols as figure 7). The curves show the effective bias of halos more massive than M_{min} (color-coded) according to Mo & White (2002) (see also Paper I). The inset is an enlargement of the low redshift area.

4.1. Redshift evolution of the bias

Figure 10 shows as symbols the redshift evolution of the bias parameter measured at 8 h^{-1} Mpc defined as $b_8 = \sigma_{8,g}/\sigma_{8,m}$ (see e.g. Magliocchetti et al. 2000) for the different samples discussed above.[4] The bias values for our *GALEX* and CFHTLS samples are reported in tables 1 and 2 respectively.

The observed bias of star-forming galaxies shows a gradual increase with look back time: at $z > 2$, UV galaxies are strongly biased (Giavalisco & Dickinson 2001; Foucaud et al. 2003), with $b_8 \gtrsim 2$, and at a given redshift the bias increases with *FUV* luminosity (*FUV* luminosity segregation). At $z \sim 1$, the mean bias is $\langle b_8 \rangle = 1.26 \pm 0.06$, indicating that star-forming galaxies are closer tracers of the underlying mass distribution at that time. At $z \leq 0.4$, given the error bars, the mean bias is consistent with 0.8 for all *GALEX* samples ($\langle b_8 \rangle = 0.79^{+0.1}_{-0.08}$), a slight anti-bias independent of the UV luminosity.

In figure 10, we also show the effective bias evolution derived from the Mo & White (2002) formalism for different minimum Dark Matter Halo (DMH) mass thresholds. A comparison can be made to the bias of star forming galaxies, if one assumes that most haloes do not host more than one star-forming galaxy. This coarse assumption is likely inaccurate for star-forming galaxies selected at high redshifts in *FUV* with a well developed one-halo term (Kashikawa et al. 2006; Lee et al. 2006), but is acceptable at low redshifts in the *FUV* since the one-halo term does not seem to play a major role as discussed sect. 3.2.

The mimimum masses of the DMH that produce the bias derived for galaxies are $10^{12}M_\odot \lesssim M \lesssim 10^{13}M_\odot$ at $z \geq 2$, $10^{11}M_\odot \lesssim M \lesssim 10^{12}M_\odot$ at $z \simeq 1$ and $M \leq 10^{12}M_\odot$ at $z < 0.4$. There is an obvious degeneracy of the models at low redshifts, but the locally observed bias is definitely in the region of low cutoff masses. This is a hint that observed star-forming galaxies at low redshift reside preferentially in less massive halos than high z star-forming galaxies.

4.2. Bias and galaxy number density

In fig. 11 we show the bias a function of the galaxy number density n_{gal} for UV-selected sam-

[4]For Adelberger et al. (2005) subsamples, δ values are not available; we assumed that the slopes are the same than those of their global samples. The expected relative error on the inferred bias is lower than 10% if $0 < \delta < 1$.

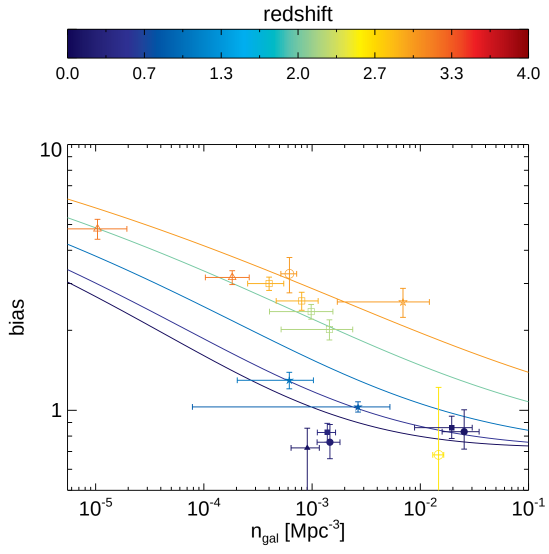

Fig. 11.— Bias of restframe UV-selected galaxies as a function of galaxy number density. The curves show the expected relation for the effective bias of Dark Matter halos at redshifts $z = 0, 0.5, 1, 2, 3$, from bottom to top. We plot only independent samples here. The legend is the same as in fig. 10.

ples and the predicted relation between the effective bias and the number density of DMHs at $z = 0, 0.5, 1, 2, 3$ (curves from bottom to top). At high redshift ($z > 1$), we observe the well known luminosity segregation effect, brighter galaxies (less abundant) having a larger bias, in good agreement with DMH models predictions (the less abundant, the more clustered). In contrast at low z ($z < 1$), a significant departure to this relation is observed. At $z \sim 0.9$, the CFHTLS data show a bias slightly lower than the expected one according to the observed density with n_{gal} approximately 3 times lower than expected. This seems even worse for our brightest samples at $z \sim 0.3$, as these galaxies are about 10 times less numerous than expected according to their bias values. In the model discussed here, we implicitly assume that one DMH hosts one galaxy, which provides a fairly reasonable description of the observations at high z, to the level of precision allowed here (see e.g. Adelberger et al. 2005; Ouchi et al. 2004, for more detailed discussions on this point). At $z < 1$, this assumption may be not valid anymore and our results suggest that star forming galaxies (especially the brightest) are not hosted by a significant fraction of the DMHs with similar clustering properties. This implies that the DMH occupation fraction, that is roughly > 0.5 at high redshift ($z > 2$), drops to 0.3 and 0.1 at $z = 1$ and $z = 0.3$ respectively.

4.3. Bias and FUV LD fraction

The very limited overlap in *FUV* luminosities of the data at different redshifts does not allow a derivation of the bias evolution with redshift at fixed *FUV* luminosity. However, despite the fact that low z samples reach fainter luminosities than high z ones, they happen to probe the same fraction of total *FUV* luminosity densities, owing to the strong evolution of the *FUV* luminosity function with z (Arnouts et al. 2005). In particular at all redshifts the samples are able to probe the bulk of star formation, *i.e.* they encompass a fraction of the *FUV* luminosity density (LD) greater than 0.5. This can be seen in fig. 12 where we show the bias as a function of the fraction of the total *FUV* LD enclosed by the different samples. This favorable situation allows us to track the evolution with redshift of the clustering at a fixed fraction of the *FUV* LD, an essentially constant fraction of the star formation rate.

The fraction of the LD for each sample is computed by comparing the total LD at the relevant redshift (from the *FUV* Luminosity function parameters of Arnouts et al. (2005) and Sawicki & Thompson (2006)), to the LD enclosed by each sample according to its flux limits converted to *FUV* luminosity cuts[5].
Note that we do not attempt to correct for galaxy internal dust attenuation. As brighter UV galaxies present higher extinction in the local Universe (Buat et al. 2005), the strong brightening of FUV_* with redshift (e.g. Arnouts et al. 2005) may introduce a small bias as a given LD fraction could not correspond exactly to the same star formation rate fraction at the different redshifts we explore here.

[5]Note that while LBG samples are by construction volume-limited, we cannot adopt this approach for the *GALEX* samples due to limited statistics. This means that faintest galaxies are underrepresented, especially in our higher redshift *GALEX* samples. However, as we do not observe a strong luminosity dependence of the bias within the *GALEX* samples, we expect this has only a small impact.

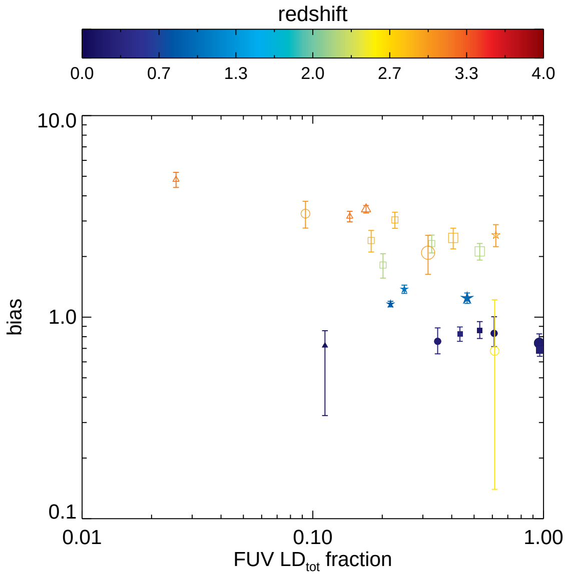

Fig. 12.— Bias of restframe *UV*-selected galaxies (symbols as in figure 10) as a function of the fraction of the FUV total luminosity density represented by each sample. The legend is the same as in fig. 10.

The plot confirms the result already apparent in fig. 10 of a significant decrease of the bias of UV selected galaxies from high to low redshifts, but now selected on the basis of a physically defined parameter, the fraction of the *FUV* luminosity density. Near an LD fraction of 0.5, the bias is divided by a factor 3, between redshifts near 3, shifting from 2.5 in the redshift range $2-3$ down to 0.8 in the local universe.

5. Discussion

In paper I we reported on the overall clustering properties of the UV-selected galaxies in *GALEX* samples, the largest ones available to date at low redshift and at these wavelengths. These samples allow for the first time an investigation of the clustering properties of UV-selected galaxies as a function of different parameters at $z \lesssim 1$, which can be compared to higher redshift samples also selected in the rest frame FUV.

The measurements from the *GALEX* samples confirm previous results for rest-UV selected galaxies at low redshifts indicating that they are weakly clustered (Heinis et al. 2004), with an auto-correlation function well approximated by a power law in the range $0.2-5$ Mpc.

At $z \sim 1$, the correlation length of the rest-UV selected galaxies from CFHTLS u' data is found comparable to those of the emission-line samples from Coil et al. (2004) in the same redshift range, but slightly higher than those obtained by Meneux et al. (2006) for late type and irregular galaxies (their types 3 and 4, selected in the visible). At those redshifts, according to our CFHTLS sample, star forming galaxies are modestly biased with $\langle b_8 \rangle = 1.26 \pm 0.06$, which under the linear bias hypothesis implies they are closer tracers of the mass distribution than their higher redshift counterparts. As opposed to the dependence found at redshifts above 2 (Giavalisco & Dickinson 2001; Foucaud et al. 2003), no strong positive correlation between the bias and the *FUV* luminosity is observed in the local universe, but rather a slight anti-correlation or no correlation. At $z \leq 0.4$, given the error bars, the mean bias is consistent with 0.8 for all *GALEX* samples ($\langle b_8 \rangle = 0.79^{+0.10}_{-0.08}$) independently of the UV luminosity.

5.1. *Migration of the bulk of star formation sites from $z = 3$ to the local universe*

In this study, we find a decrease by a factor 3.1 of the bias with respect to mass, from redshifts near 3 to the local universe in the UV flux-limited samples, and more importantly in samples selected in UV luminosity so that they encompass a constant fraction of the luminosity density at all z. This decrease is slightly larger than the factor 2.7 derived from the Mo & White (2002) model for the $M \geq 10^{12} M_\odot$ haloes that host most star formation at redshift 3, an indication that star forming galaxies tend to be hosted by haloes of lower mass in the local universe. This is the main conclusion of the present study.

The "downsizing" scenario (Cowie et al. 1996; Juneau et al. 2005; Bundy et al. 2005; Heavens et al. 2004) states that the star formation shifts from high stellar mass systems at high redshift to low ones at low redshift. Our results extend this vision in the sense that the same trend is observed for the mass of the dark matter halos that host actively star forming galaxies.

The DMH mass migration of the bulk of the star formation might be associated with regions of different densities. At high redshifts, LBGs studies show that active star formation traced by the UV light resides preferentially in overdense regions (Adelberger et al. 1998; Blaizot et al. 2004; Giavalisco 2002; Steidel et al. 1998; Tasker & Bryan 2006). At low redshift, Abbas & Sheth (2005) showed that the slope of the fitted power law is steeper in underdense regions, and that the correlation length is smaller. The observed steeper ACFs for the more UV-luminous galaxies at low z suggest that the most star-forming objects reside preferentially in regions where the local galaxy density is lower than for the fainter ones, a result in agreement with direct optical based studies of star formation as a function of galaxy density in the local universe (Gómez et al. 2003; Lewis et al. 2002).

We thank Christian Marinoni for stimulating discussions.

GALEX (Galaxy Evolution Explorer) is a NASA Small Explorer, launched in April 2003. We gratefully acknowledge NASA's support for construction, operation, and science analysis for the *GALEX* mission, developed in cooperation with the Centre National d'Etudes Spatiales of France and the Korean Ministry of Science and Technology.

This study is also based on observations obtained with MegaPrime/MegaCam, a joint project of CFHT and CEA/DAPNIA, at the Canada-France-Hawaii Telescope (CFHT) which is operated by the National Research Council (NRC) of Canada, the Institut National des Science de l'Univers of the Centre National de la Recherche Scientifique (CNRS) of France, and the University of Hawaii. This work is based in part on data products produced at TERAPIX and the Canadian Astronomy Data Centre as part of the Canada-France-Hawaii Telescope Legacy Survey, a collaborative project of NRC and CNRS.

REFERENCES

Abbas, U., & Sheth, R. K. 2005, MNRAS, 364, 1327

Adelberger, K. L., Steidel, C. C., Giavalisco, M., Dickinson, M., Pettini, M., & Kellogg, M. 1998, ApJ, 505, 18

Adelberger, K. L., Steidel, C. C., Pettini, M., Shapley, A. E., Reddy, N. A., & Erb, D. K. 2005, ApJ, 619, 697

Allen, P. D., Moustakas, L. A., Dalton, G., MacDonald, E., Blake, C., Clewley, L., Heymans, C., & Wegner, G. 2005, MNRAS, 360, 1244

Arnouts, S., et al. 2002, MNRAS, 329, 355

Arnouts, S., et al. 2005, ApJ, 619, L43

Arnouts, S., & Ilbert, 0. in preparation

Baldry, I. K., Glazebrook, K., Brinkmann, J., Ivezić, Ž., Lupton, R. H., Nichol, R. C., & Szalay, A. S. 2004, ApJ, 600, 681

Benoist, C., Maurogordato, S., da Costa, L. N., Cappi, A., & Schaeffer, R. 1996, ApJ, 472, 452

Benson, A. J., Frenk, C. S., Baugh, C. M., Cole, S., & Lacey, C. G. 2001, MNRAS, 327, 1041

Benson, A. J., Bower, R. G., Frenk, C. S., Lacey, C. G., Baugh, C. M., & Cole, S. 2003, ApJ, 599, 38

Berlind, A. A., et al. 2003, ApJ, 593, 1

Blaizot, J., Guiderdoni, B., Devriendt, J. E. G., Bouchet, F. R., Hatton, S. J., & Stoehr, F. 2004, MNRAS, 352, 571

Buat, V., et al. 2005, ApJ, 619, L51

Budavári, T., et al. 2003, ApJ, 595, 59

Bundy, K., et al. 2005, ArXiv Astrophysics e-prints, arXiv:astro-ph/0512465

Burgarella, D., et al. 2006, A&A, 450, 69

Cardelli, J. A., Clayton, G. C., & Mathis, J. S. 1989, ApJ, 345, 245

Cattaneo, A., Dekel, A., Devriendt, J., Guiderdoni, B., & Blaizot, J. 2006, MNRAS, 370, 1651

Coil, A. L., et al. 2004, ApJ, 609, 525

Connolly, A. J., Csabai, I., Szalay, A. S., Koo, D. C., Kron, R. G., & Munn, J. A. 1995, AJ, 110, 2655

Cowie, L. L., Songaila, A., Hu, E. M., & Cohen, J. G. 1996, AJ, 112, 839

Cross, N., et al. 2001, MNRAS, 324, 825

Croton, D. J., et al. 2006, MNRAS, 365, 11

Foucaud, S., McCracken, H. J., Le Fèvre, O., Arnouts, S., Brodwin, M., Lilly, S. J., Crampton, D., & Mellier, Y. 2003, A&A, 409, 835

Giavalisco, M., & Dickinson, M. 2001, ApJ, 550, 177

Giavalisco, M. 2002, ARA&A, 40, 579

Gómez, P. L., et al. 2003, ApJ, 584, 210

Guzzo, L., et al. 2000, A&A, 355, 1

Heavens, A., Panter, B., Jimenez, R., & Dunlop, J. 2004, Nature, 428, 625

Heinis, S., Treyer, M., Arnouts, S., Milliard, B., Donas, J., Gal, R., Martin, D. C., & Viton, M. 2004, A&A, 424, L9

Hopkins, A. M. 2004, ApJ, 615, 209

Ilbert, O., et al. 2006, A&A, 457, 841

Jimenez, R., Panter, B., Heavens, A. F., & Verde, L. 2005, MNRAS, 356, 495

Juneau, S., et al. 2005, ApJ, 619, L135

Kashikawa, N., et al. 2006, ApJ, 637, 631

Kereš, D., Katz, N., Weinberg, D. H., & Davé, R. 2005, MNRAS, 363, 2

Kravtsov, A. V., Berlind, A. A., Wechsler, R. H., Klypin, A. A., Gottlöber, S., Allgood, B., & Primack, J. R. 2004, ApJ, 609, 35

Landy, S. D., & Szalay, A. S. 1993, ApJ, 412, 64

Lee, K.-S., Giavalisco, M., Gnedin, O. Y., Somerville, R. S., Ferguson, H. C., Dickinson, M., & Ouchi, M. 2006, ApJ, 642, 63

Le Fèvre, O., et al. 2005, A&A, 439, 845

Lewis, I., et al. 2002, MNRAS, 334, 673

Lilly, S. J., Le Fevre, O., Hammer, F., & Crampton, D. 1996, ApJ, 460, L1

Madau, P., Ferguson, H. C., Dickinson, M. E., Giavalisco, M., Steidel, C. C., & Fruchter, A. 1996, MNRAS, 283, 1388

Madgwick, D. S., et al. 2002, MNRAS, 333, 133

Magliocchetti, M., Bagla, J. S., Maddox, S. J., & Lahav, O. 2000, MNRAS, 314, 546

Magliocchetti, M., & Porciani, C. 2003, MNRAS, 346, 186

Marinoni, C., et al. 2005, A&A, 442, 801

McCracken, H. J., et al. 2003, A&A, 410, 17

Meneux, B., et al. 2006, A&A, 452, 387

Milliard, B., Heinis, S., Arnouts, S., Blaizot, J., Schiminovich, D., Budavári, T., Donas, J., Treyer, M., Wyder, T. K., & GALEX Team 2006, ApJ, submitted

Mo, H. J., & White, S. D. M. 2002, MNRAS, 336, 112

Norberg, P., et al. 2001, MNRAS, 328, 64

Norberg, P., et al. 2002, MNRAS, 332, 827

Ouchi, M., et al. 2001, ApJ, 558, L83

Ouchi, M., et al. 2004, ApJ, 611, 685

Ouchi, M., et al. 2005, ApJ, 635, L117

Peebles, P. J. E. 1980, Princeton University Press

Reddy, N. A., Steidel, C. C., Fadda, D., Yan, L., Pettini, M., Shapley, A. E., Erb, D. K., & Adelberger, K. L. 2006, ApJ, 644, 792

Roberts, S., et al. 2004, MNRAS, 352, 478

Roche, N., & Eales, S. A. 1999, MNRAS, 307, 703

Sawicki, M., & Thompson, D. 2006, ApJ, 642, 653

Schiminovich, D., et al. 2005, ApJ, 619, L47

Schlegel, D. J., Finkbeiner, D. P., & Davis, M. 1998, ApJ, 500, 525

Schultheis, M., Robin, A. C., Reylé, C., McCracken, H. J., Bertin, E., Mellier, Y., & Le Fèvre, O. 2006, A&A, 447, 185

Steidel, C. C., Adelberger, K. L., Dickinson, M., Giavalisco, M., Pettini, M., & Kellogg, M. 1998, ApJ, 492, 428

Sullivan, M., Treyer, M. A., Ellis, R. S., Bridges, T. J., Milliard, B., & Donas, J. 2000, MNRAS, 312, 442

Tasker, E. J., & Bryan, G. L. 2006, ArXiv Astrophysics e-prints, arXiv:astro-ph/0603684

Willmer, C. N. A., da Costa, L. N., & Pellegrini, P. S. 1998, AJ, 115, 869

Wilson, G., Cowie, L. L., Barger, A. J., & Burke, D. J. 2002, AJ, 124, 1258

Zehavi, I., et al. 2002, ApJ, 571, 172

Zehavi, I., et al. 2004, ApJ, 608, 16

Zehavi, I., et al. 2005, ApJ, 630, 1